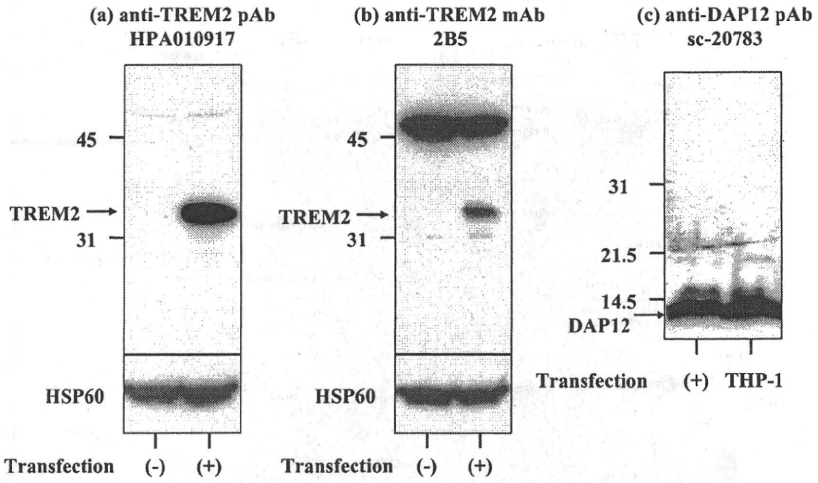

Fig. 3 Validation of antibody specificity by Western blot. The open-reading frame of the human triggering receptor expressed on myeloid cells 2 (TREM2) or DNAX-activation protein 12 (DAP12) gene was cloned in the expression vector pEF6-TOPO, and was transfected in HEK293 cells to express a nontagged recombinant TREM2 or DAP12 protein. Then, the protein extract was processed for Western blot analysis. The panels represent: (a) TREM2-expressing cells with anti-TREM2 pAb (HPA010917); (b) TREM2-expressing cells with anti-TREM2 mAb (2B5); and (c) DAP12-expressing cells with anti-DAP12 pAb (sc-20783). The blots in (a) and (b) were reprobed with anti-HSP60 antibody for an internal control (lower panels). The lanes indicate (–) nontransfected cells and (+) transfected cells. The left lane of the panel (c) represents the protein extract of THP-1 human monocytic leukemia cell line, serving as a positive control. It is evident that the anti-TREM2 mAb (2B5) reacts with a 47-kDa non-TREM2 protein (panel b).

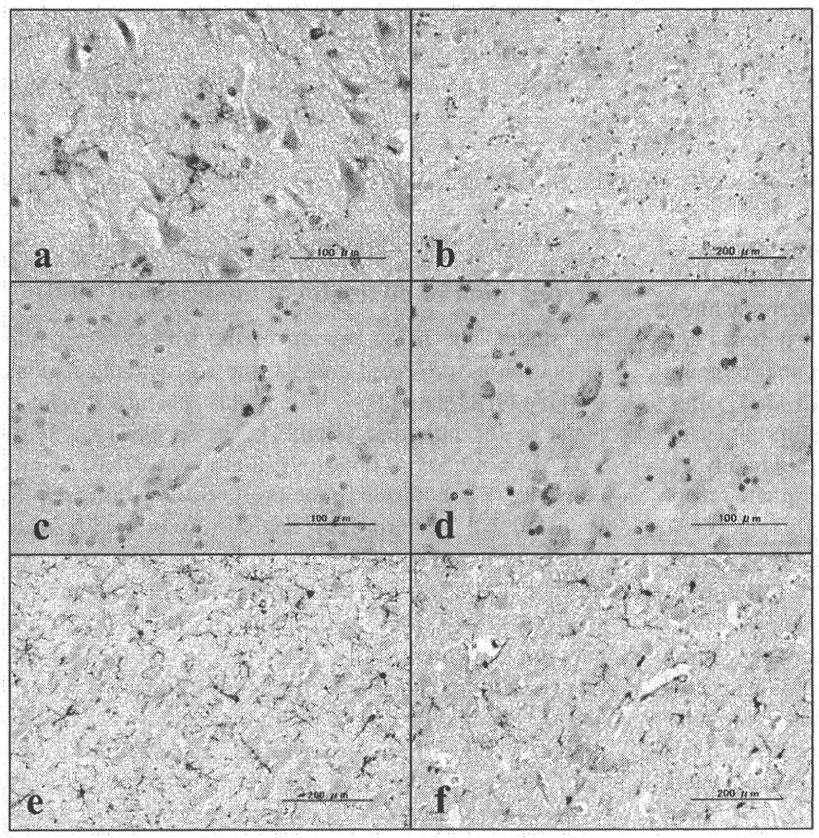

Fig. 4 DNAX-activation protein 12 (DAP12), triggering receptor expressed on myeloid cells 2 (TREM2), and Iba1 expression in Nasu-Hakola disease (NHD) and control brains. Formalin-fixed paraffin-embedded tissue sections of three NHD, four myotonic dystrophy (MD), and four non-neurological control (NC) brains were processed for immunohistochemistry with antibodies listed in Table 1. The panels represent: (a) NC1, the frontal cortex, DAP12; (b) NHD2, the basal ganglia, DAP12; (c) NC1, the frontal white matter, TREM2; (d) NHD3, the frontotemporal cortex, TREM2; (e) NC2, the hippocampus, Iba1; and (f) NHD1, the hippocampus, Iba1.

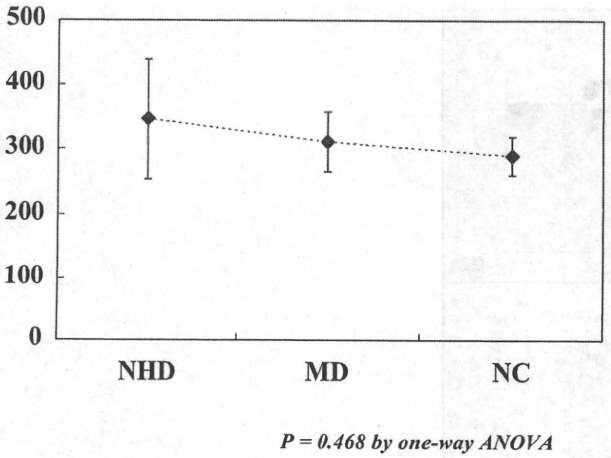

Fig. 5 Iba1-positive microglia are preserved in the frontal cortex of Nasu-Hakola disease (NHD). The sum of Iba1-positive cells in three fields of the frontal cortex where the layer III is centered at a 200× magnification was counted in each case. The average and standard deviation are shown. No statistically significant difference was observed among NHD ($n = 3$), myotonic dystrophy (MD) ($n = 4$), and non-neurological control (NC) ($n = 4$) cases evaluated by one-way analysis of variance ($P = 0.468$).

Iba1 (AIF1) is identified as one of the NHD-specific biomarkers by bioinformatics analysis of NHD DC transcriptome. We identified an intense Iba1 immunoreactivity on virtually all of microglia and macrophages distributed in the cortex and the white matter of control and NHD brains (Fig. 4e,f). The number of Iba1-positive cells in the frontal cortex was not significantly different among NHD, MD and NC brains (Fig. 5), indicating that DAP12-deficient microglia are well preserved in NHD brains. Less than half of Iba1-immunoreactive microglia and macrophages intensely expressed human leukocyte antigen MHC class II DR (HLA-DR), located chiefly in the white matter in control and NHD brains, whereas astrocytes, oligodendrocytes and neurons were negative for HLA-DR (Fig. 6a–d). A substantial subset of microglia and macrophages also expressed CD68 in all the brains examined, where CD68-positive giant and bizarre macrophages, possibly phagocytosing tissue debris, were found more often in NHD brains (Fig. 6e,f). CD163 and MSR1 were expressed chiefly on some populations of perivascular macrophages and occasionally on a small subset of microglia in control and NHD brains (Fig. 7a–d), while SIGLEC1 was expressed exclusively on an extremely small subset of perivascular mac-

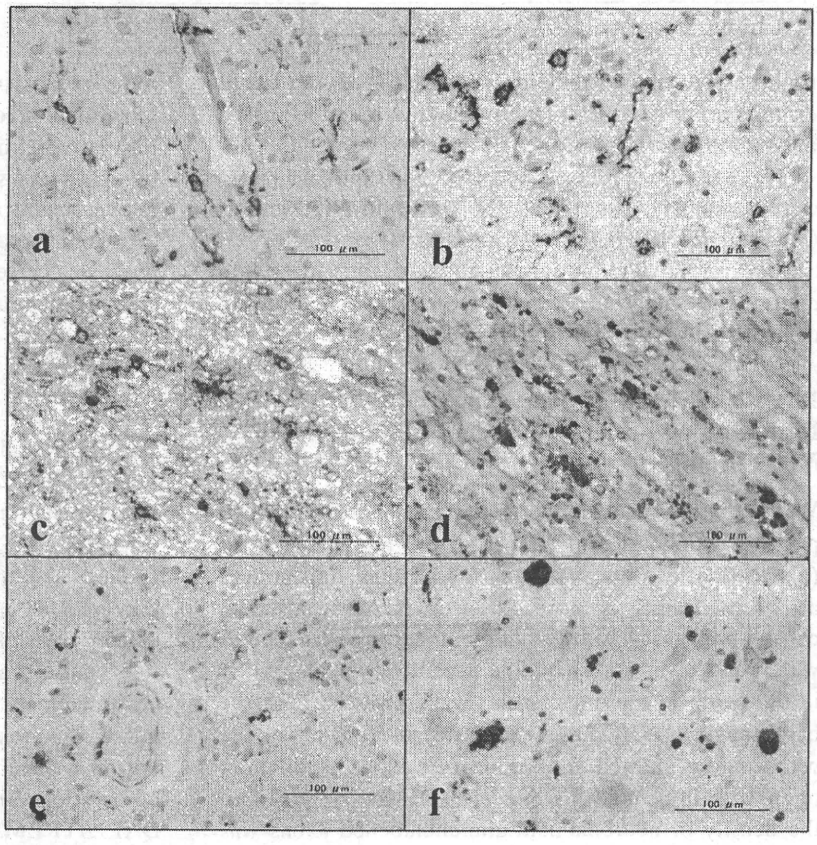

Fig. 6 Human leukocyte antigen MHC class II DR (HLA-DR), Iba1 and CD68 expression in Nasu-Hakola disease (NHD) and control brains. The panels represent: (a) non-neurological control (NC)2, the frontal white matter, HLA-DR; (b) NHD3, the periventricular white matter of the hippocampus, HLA-DR; (c) myotonic dystrophy (MD)1, the frontal white matter, HLA-DR (red) and Iba1 (brown); (d) NHD2, the basal ganglia, HLA-DR (red) and Iba1 (brown); (e) NC2, the frontal white matter, CD68; and (f) NHD3, the hippocampus, CD68.

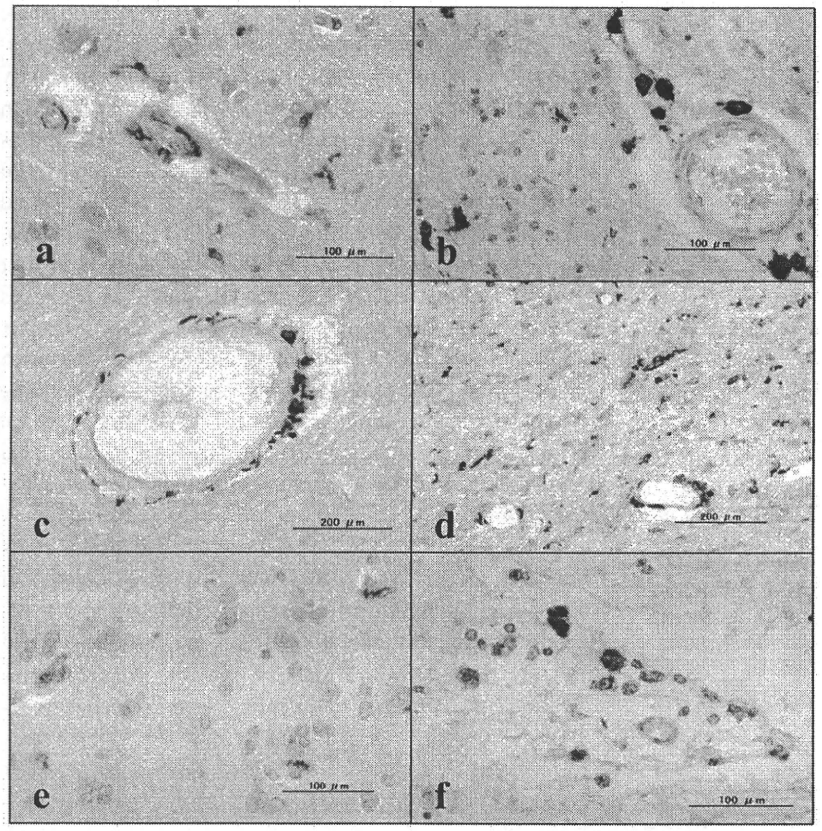

Fig. 7 CD163, MSR1, and sialic acid binding Ig-like lectin 1 (SIGLEC1) expression in Nasu-Hakola disease (NHD) and control brains. The panels represent: (a) myotonic dystrophy (MD)4, the frontal cortex, CD163; (b) NHD3, the frontal white matter, CD163; (c) MD3, the frontal white matter, MSR1; (d) NHD2, the basal ganglia, MSR1; (e) MD4, the frontal cortex, SIGLEC1, and; (f) NHD3, the frontal white matter, SIGLEC1.

rophages but undetectable on microglia in all the brains examined, and SIGLEC1-positive cells were not increased in NHD brains (Fig. 7e,f).

TREM1 was expressed on multipolar fibrillary astrocytes located in the cortex of control and NHD brains (Fig. 8a,b). SIRPB1 was expressed chiefly on small-sized astrocytes located in the subpial and periventricular white matter and small subsets of microglia and neurons in control and NHD brains (Fig. 8c,d).

Intense astrogliosis, demyelination, spheroid formation and calcosphere deposition in NHD brains

We identified a small number of perivascular cuffs of CD3-positive lymphocytes in almost all the brains examined (Fig. 8e,f). The white matter showed diffuse and intense astrogliosis, which is more severe in NHD brains than control brains (Fig. 9a,b). Notably, numerous calcospheres with round, ovoid and chain-like structures were deposited in the parenchyma and vascular walls, exclusively in the basal ganglia of NHD brains (Fig. 9c,d). In NHD brains, the white matter showed varying degrees of demyelination, often with ill-defined margins (Fig. 9f). In NHD brains, the density of neurofilament-immunolabelled axons was reduced substantially in the white matter, accompanied by accumulation of numerous axonal spheroids (Fig. 10b). Furthermore, only in the NHD3 brain but not in other brains, a very small subset of neurons expressed intense immunoreactivity for cleaved caspase 3, a marker of ongoing apoptosis (Fig. 10d). Synaptophysin immunoreactivity was preserved in NHD brains regardless of noticeable loss of neurons (Fig. 10f).

DISCUSSION

Nasu-Hakola disease is caused by loss-of-function mutations of DAP12 or TREM2.[6,7] TREM2 and DAP12 constitute a receptor/adapter signaling complex expressed on osteoclasts, DC, macrophages and microglia.[14–16] Previous studies using mouse models showed that the number of microglia is greatly reduced in the brain of DAP12-deficient/loss-of-function mice associated with demyelination and synaptic degeneration[9,11–13] and NHD is attributable to the inability of DAP12/TREM2-deficient microglia to remove apoptotic neurons, followed by induction of a pro-inflammatory milieu in the brain.[10,19] These observations led to the proposal that a loss-of-function of DAP12/TREM2 in microglia plays a central role in devel-

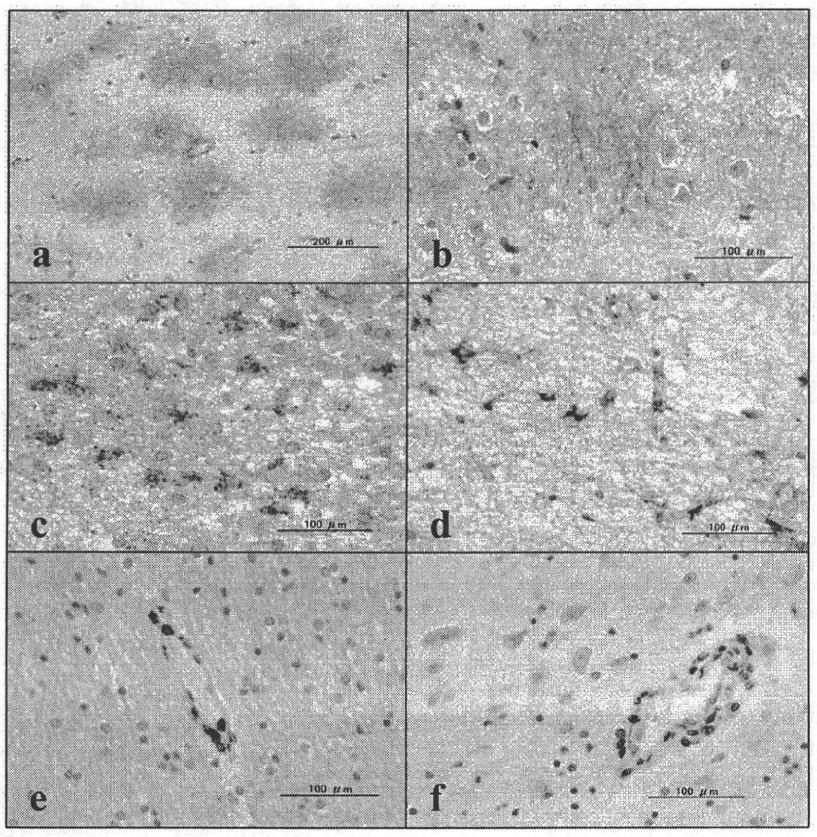

Fig. 8 Triggering receptor expressed on myeloid cells 1 (TREM1), signal-regulatory protein beta 1 (SIRPB1), and CD3 expression in Nasu-Hakola disease (NHD) and control brains. The panels represent: (a) non-neurological control (NC)3, the temporal cortex, TREM1; (b) NHD3, the basal ganglia, TREM1; (c) myotonic dystrophy (MD)3, the white matter close to the hippocampus, SIRPB1; (d) NHD1, the periventricular white matter close to the basal ganglia, SIRPB1; (e) NC3, the frontal white matter, CD3; and (f) NHD3, the frontotemporal cortex, CD3.

opment of the neuropathology of NHD. However, there exist no immunohistochemical studies that have focused on microglia in NHD brains.

In the present study, first, we identified a set of 73 genes deregulated in NHD patients by bioinformatics analysis of genome-wide transcriptome data of DC. The panel of 73 DEGs constitutes a highly complex molecular network closely related to inflammatory response, cell signaling, and molecular transport. From 73 DEGs, we extracted six genes upregulated in DC of both DAP12-mutated and TREM2-mutated patients. They include AIF1 (Iba1), MS4A6A, ITPR2, SIGLEC1, RAP2B and CTBP2, serving as a candidate for NHD-specific biomarker molecules. Among them, we selected Iba1 and SIGLEC1 for immunohistochemical analysis, because it is well known that Iba1 is a microglia/macrophage-specific calcium-binding protein that regulates the Rac GTPase-dependent membrane ruffling and phagocytosis.[22] SIGLEC1 (sialoadhesin, CD169) is a receptor for N-acetylneuraminic acid (Neu5Ac) expressed on activated microglia.[23]

In the second step, we studied three NHD, four MD, and four NC brains by immunohistochemistry with a panel of 16 different antibodies, including those against Iba1 and SIGLEC1. We validated the absence of DAP12 expression in NHD brains and the presence of DAP12 immunoreactivity on ramified microglia in control brains. In contrast to the previous studies,[14–16] we could not detect TREM2 expression on microglia in any brains examined, but we found TREM2 expression on a small subset of intravascular monocytes/macrophages in all the brains examined. Most importantly, we identified accumulation of numerous Iba1-positive microglia in the cortex of NHD to an extent similar to control brains. SIGLEC1 was undetectable on microglia in all the brains examined. Although we identified Iba1 and SIGLEC1 as putative NHD-specific biomarkers by bioinformatics analysis of DC transcriptome, we concluded that these NHD DC-derived biomarkers do not reflect effectively the pathological condition of microglia directly relevant to development of NHD brain lesions. The present observations indicated that DAP12-deficient microglia that do not express TREM2 are preserved in NHD brains. Consistent with our results, a previous study showed widespread activation of CD68-immunoreactive microglia in the cerebral white matter of NHD brains.[24]

Previous studies showed that TREM2 is expressed in osteoclasts, macrophages, dendritic cells, and microglia.[14–16] *In vivo* TREM2 is localized to a subset of mouse microglia detected by *in situ* hybridization and by immunohis-

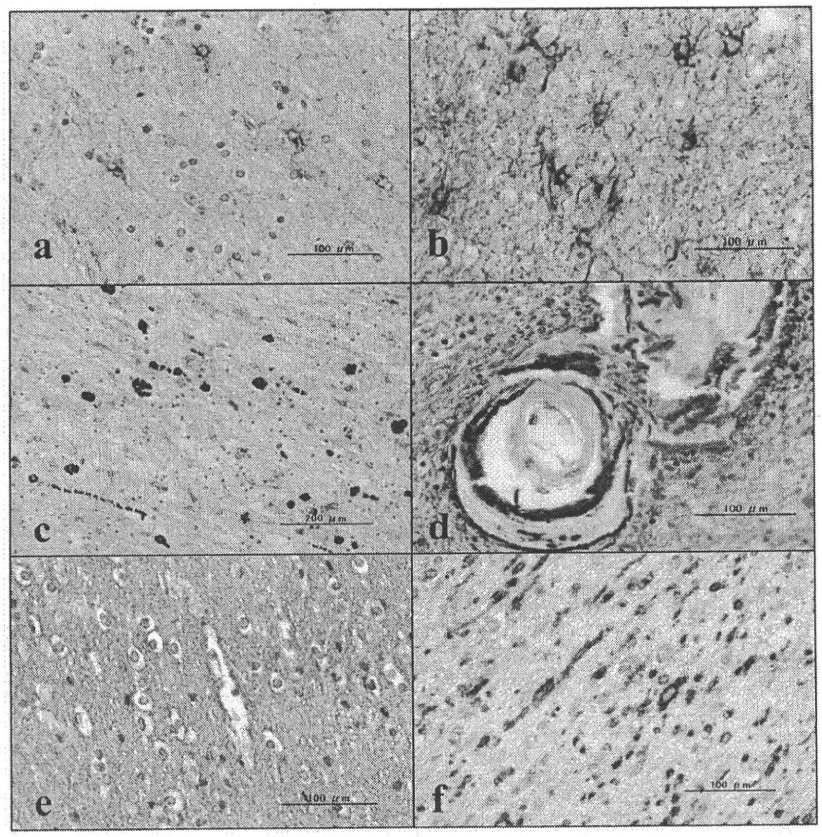

Fig. 9 GFAP and MBP expression in Nasu-Hakola disease (NHD) and control brains. The panels represent: (a) non-neurological control (NC)4, the frontal white matter, GFAP; (b) NHD1, the frontal white matter, GFAP; (c) NHD1, the basal ganglia, GFAP; (d) NHD2, the basal ganglia, GFAP; (e) NC2, the frontal white matter, MBP; and (f) NHD3, the frontal white matter, MBP.

tochemistry.[25] In the human and mouse cerebral cortex, microglia along with a subset of neurons coexpress TREM2 and DAP12, although microglial TREM2 is mainly located intracellularly in the Golgi complex/*trans*-Goligi network and exocytic vesicles.[15,26] TREM2, by interacting with plexin-A1, a receptor for Sema6D that plays a key role in axonal guidance, links the semaphorin-signaling pathway to the DAP12 signaling pathway.[27] TREM2 is not expressed on resting macrophages but is induced on activated macrophages that infiltrate the tissues from the circulation.[28] TREM2 is expressed intensely on a subset of CSF monocytes and myelin-laden macrophages in active demyelinating lesions of MS, whereas microglia express very weak immunoreactivity for TREM2 in the normal-appearing white matter of MS brains.[29] In contrast to previous observations,[14–16] we found that TREM2 is undetectable on microglia in NHD and control brain tissues. The possibility could not be excluded that these discrepancies are attributable to differences in the species, either human or mouse, the stage of the underlying pathology, and the quality of antibodies examined. These studies, except for our own, validated the antibody specificity by Western blot. We tested four different anti-TREM2 antibodies available commercially, such as HPA010917 (Sigma), 2B5 (Novus Biologicals), ab69405 (Abcam), and ab69868 (Abcam). However, only the antibody HPA010917 satisfied the specificity and the reactivity to human TREM2 protein (Fig. 3a,b, and other data not shown). Furthermore, we found TREM2 expression on a small subset of intravascular monocytes/macrophages in all the brains examined, suggesting that the anti-TREM2 antibody HPA010917 works well on formalin-fixed, paraffin-embedded tissue sections.

TREM2 expression is rapidly downregulated in macrophages and microglia by exposure to LPS or IFN-γ.[14,28] TREM2 is upregulated on macrophages and microglia in the lesions of experimental autoimmune encephalomyelitis (EAE), and blockade of TREM2 enhances inflammatory demyelination during the effector phase of EAE.[30] The levels of TREM2 expression are elevated in microglia that accumulate around amyloid plaques in aged APP23 transgenic mice.[31] All of these observations suggest that TREM2 expression on microglia *in situ* could be transient, depending on the pathological environments.

A previous study showed that SIRPB1 expressed on microglia is involved in phagocytosis of amyloid-β in Alzheimer disease (AD) brains.[32] However, we found that SIRPB1 and TREM1, capable of serving as alternative

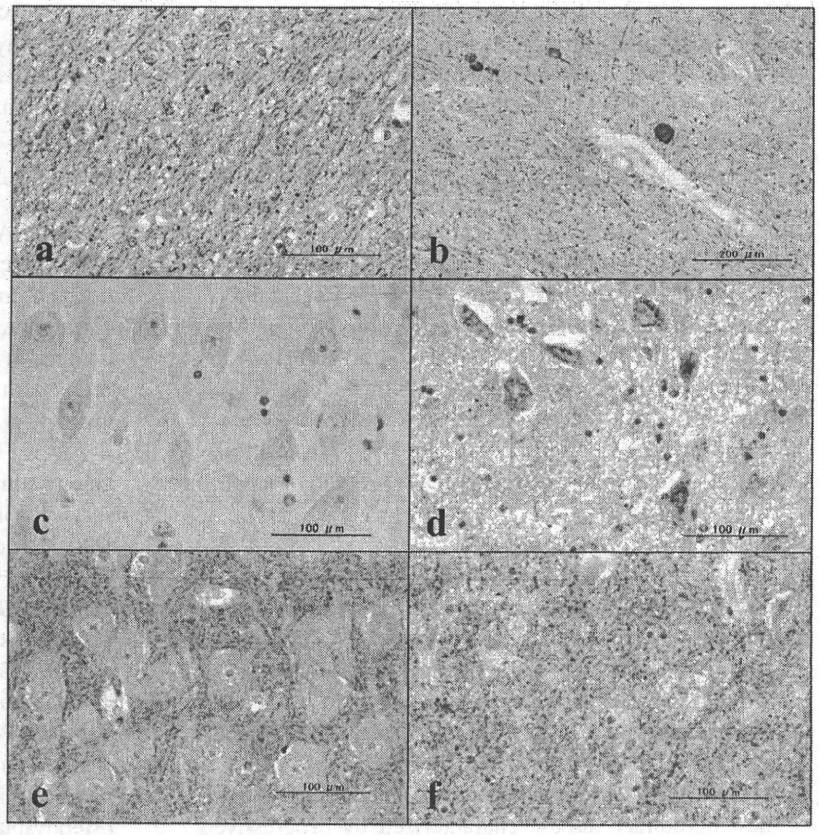

Fig. 10 Neurofilament protein, cleaved caspase-3, and synaptophysin expression in Nasu-Hakola disease (NHD) and control brains. The panels represent: (a) non-neurological control (NC)4, the frontal white matter, neurofilament (NF); (b) NHD2, the frontal white matter, NF; (c) NC4, the hippocampus, cleaved caspase-3; (d) NHD3, the hippocampus, cleaved caspase-3; (e) NC2, the hippocampus, synaptophysin (SYNAP); and (f) NHD3, the hippocampus, SYNAP.

DAP12-binding partners, were expressed chiefly on a small population of astrocytes in both NHD and control brains, not excluding their role in astroglial pathology in NHD. CD163 and MSR1 were expressed chiefly on a population of perivascular macrophages and some microglia. CD163 is a glycoprotein that belongs to the scavenger receptor cysteine-rich (SRCR) family group B. CD163 acts as a cell-surface scavenger receptor capable of internalizing the haptoglobin–hemoglobin complex for clearance of the potent oxidant hemoglobin from the circulation.[33] MSR1 (CD204) is the scavenger receptor class A (SR-A) that mediates the endocytosis of modified low-density lipoproteins (LDLs). The expression of MSR1 is enhanced on microglia in AD brains.[34] It is worthy to note that CD68-positive macrophages with a giant and bizarre morphology accumulated more often in NHD brains. They might correspond to the cells positive for sudanophilic granules described previously.[4,5] These observations suggest the possible scenario that DAP12-deficient macrophages that accumulate in NHD brains are capable of taking up tissue debris but incapable of efficiently digesting them.

Finally, consistent with previous studies,[4,5] we found that NHD brain lesions were characterized by intense astrogliosis, diffuse demyelination, axonal loss and accumulation of axonal spheroids and numerous calcospheres. A previous study classified the pattern of intracranial calcification in neurodegenerative diseases into three types of distinct generation: diffuse deposition within the tunica media of small and medium-sized vessels (type 1), free spherical or lobulated concretions in the parenchyma (type 2), and rows of small calcosherites locating along the capillaries (type 3).[35] We identified all three types of calcification in the basal ganglia of NHD brains. It is worthy to note that we often identified type 3 calcification, the hallmark of the most severe intracranial calcification, in NHD brains.

In summary, we found that TREM2 is undetectable on microglia in all the brains examined and DAP12-deficient microglia are well preserved in NHD brains. These observations suggest that the loss of DAP12/TREM2 function in microglia might not be primarily responsible for development of the neuropathological manifestation of NHD. In line with this view, NHD patients do not exhibit any obvious immunological defects despite the complete loss of DAP12/TREM2 function in immune cells, but shows severe defects in bone remodeling due to impaired differentiation and maturation of osteoclasts.[3] Therefore, we

could propose the possible scenario that extracranial factors, such as long-term disturbance of calcium homeostasis, might affect neuronal and glial function, resulting in induction of the CNS pathology of NHD.

ACKNOWLEDGMENTS

The authors would thank Research Resource Network (RRN), Tokyo, Japan for providing us human brain tissues. This work was supported by grants from the Research on Intractable Diseases, the Ministry of Health, Labour and Welfare of Japan, entitled Clinicopathological and Genetic Studies of Nasu-Hakola disease (H22-Nanchi-Ippan-136), and the High-Tech Research Center Project (S0801043) and the Grant-in-Aid (C22500322), the Ministry of Education, Culture, Sports, Science and Technology (MEXT) of Japan.

REFERENCES

1. Nasu T, Tsukahara Y, Terayama K. A lipid metabolic disease – "Membranous lipodystrophy" – an autopsy case demonstrating numerous peculiar membrane-structures composed of compound lipid in bone and bone marrow and various adipose tissues. *Acta Pathol Jpn* 1973; **23**: 539–558.
2. Hakola HP. Neuropsychiatric and genetic aspects of a new hereditary disease characterized by progressive dementia and lipomembranous polycystic osteodysplasia. *Acta Psychiatr Scand Suppl* 1972; **232**: 1–173.
3. Bianchin MM, Capella HM, Chaves DL *et al.* Nasu-Hakola disease (polycystic lipomembranous osteodysplasia with sclerosing leukoencephalopathy – PLOSL): a dementia associated with bone cystic lesions. From clinical to genetic and molecular aspects. *Cell Mol Neurobiol* 2004; **24**: 1–24.
4. Tanaka J. Nasu-Hakola disease: a review of its leukoencephalopathic and membranolipodystrophic features. *Neuropathology* 2000; **20**: S25–S29.
5. Kaneko M, Sano K, Nakayama J, Amano N. Nasu-Hakola disease: the first case reported by Nasu and review. *Neuropathology* 2010; **30**: 463–470. DOI: 10.1111/j.1440-1789.2010.01127.x.
6. Paloneva J, Manninen T, Christman G *et al.* Mutations in two genes encoding different subunits of a receptor signaling complex result in an identical disease phenotype. *Am J Hum Genet* 2002; **71**: 656–662.
7. Klünemann HH, Ridha BH, Magy L *et al.* The genetic causes of basal ganglia calcification, dementia, and bone cysts: DAP12 and TREM2. *Neurology* 2005; **64**: 1502–1507.
8. Turnbull IR, Colonna M. Activating and inhibitory functions of DAP12. *Nat Rev Immunol* 2007; **7**: 155–161.
9. Kaifu T, Nakahara J, Inui M *et al.* Osteopetrosis and thalamic hypomyelinosis with synaptic degeneration in DAP12-deficient mice. *J Clin Invest* 2003; **111**: 323–332.
10. Hamerman JA, Tchao NK, Lowell CA, Lanier LL. Enhanced Toll-like receptor responses in the absence of signaling adaptor DAP12. *Nat Immunol* 2005; **6**: 579–586.
11. Roumier A, Béchade C, Poncer JC *et al.* Impaired synaptic function in the microglial KARAP/DAP12-deficient mouse. *J Neurosci* 2004; **24**: 11421–11428.
12. Nataf S, Anginot A, Vuaillat C *et al.* Brain and bone damage in KARAP/DAP12 loss-of-function mice correlate with alterations in microglia and osteoclast lineages. *Am J Pathol* 2005; **166**: 275–286.
13. Otero K, Turnbull IR, Poliani PL *et al.* Macrophage colony-stimulating factor induces the proliferation and survival of macrophages via a pathway involving DAP12 and beta-catenin. *Nat Immunol* 2009; **10**: 734–743.
14. Schmid CD, Sautkulis LN, Danielson PE *et al.* Heterogeneous expression of the triggering receptor expressed on myeloid cells-2 on adult murine microglia. *J Neurochem* 2002; **83**: 1309–1320.
15. Sessa G, Podini P, Mariani M *et al.* Distribution and signaling of TREM2/DAP12, the receptor system mutated in human polycystic lipomembraneous osteodysplasia with sclerosing leukoencephalopathy dementia. *Eur J Neurosci* 2004; **20**: 2617–1628.
16. Thrash JC, Torbett BE, Carson MJ. Developmental regulation of TREM2 and DAP12 expression in the murine CNS: implications for Nasu-Hakola disease. *Neurochem Res* 2009; **34**: 38–45.
17. Stefano L, Racchetti G, Bianco F *et al.* The surface-exposed chaperone, Hsp60, is an agonist of the microglial TREM2 receptor. *J Neurochem* 2009; **110**: 284–294.
18. Hsieh CL, Koike M, Spusta SC *et al.* A role for TREM2 ligands in the phagocytosis of apoptotic neuronal cells by microglia. *J Neurochem* 2009; **109**: 1144–1156.
19. Takahashi K, Rochford CD, Neumann H. Clearance of apoptotic neurons without inflammation by microglial triggering receptor expressed on myeloid cells-2. *J Exp Med* 2005; **201**: 647–657.
20. Kiialainen A, Veckman V, Saharinen J *et al.* Transcript profiles of dendritic cells of PLOSL patients link demyelinating CNS disorders with abnormalities in pathways of actin bundling and immune response. *J Mol Med* 2007; **85**: 971–983.
21. Satoh JI, Tabunoki H, Yamamura T. Molecular network of the comprehensive multiple sclerosis brain-lesion proteome. *Mult Scler* 2009; **15**: 531–541.
22. Imai Y, Kohsaka S. Intracellular signaling in M-CSF-induced microglia activation: role of Iba1. *Glia* 2002; **40**: 164–174.

23. Perry VH, Crocker PR, Gordon S. The blood-brain barrier regulates the expression of a macrophage sialic acid-binding receptor on microglia. *J Cell Sci* 1992; **101**: 201–207.
24. Paloneva J, Autti T, Raininko R *et al.* CNS manifestations of Nasu-Hakola disease: a frontal dementia with bone cysts. *Neurology* 2001; **56**: 1552–1558.
25. Schmid CD, Melchior B, Masek K *et al.* Differential gene expression in LPS/IFNgamma activated microglia and macrophages: in vitro versus in vivo. *J Neurochem* 2009; **109** (Suppl 1): 117–125.
26. Prada I, Ongania GN, Buonsanti C, Panina-Bordignon P, Meldolesi J. Triggering receptor expressed in myeloid cells 2 (TREM2) trafficking in microglial cells: continuous shuttling to and from the plasma membrane regulated by cell stimulation. *Neuroscience* 2006; **140**: 1139–1148.
27. Takegahara N, Takamatsu H, Toyofuku T *et al.* Plexin-A1 and its interaction with DAP12 in immune responses and bone homeostasis. *Nat Cell Biol* 2006; **8**: 615–622.
28. Turnbull IR, Gilfillan S, Cella M *et al.* Cutting edge: TREM-2 attenuates macrophage activation. *J Immunol* 2006; **177**: 3520–3524.
29. Piccio L, Buonsanti C, Cella M *et al.* Identification of soluble TREM-2 in the cerebrospinal fluid and its association with multiple sclerosis and CNS inflammation. *Brain* 2008; **131**: 3081–3091.
30. Piccio L, Buonsanti C, Mariani M *et al.* Blockade of TREM-2 exacerbates experimental autoimmune encephalomyelitis. *Eur J Immunol* 2007; **37**: 1290–1301.
31. Frank S, Burbach GJ, Bonin M *et al.* TREM2 is upregulated in amyloid plaque-associated microglia in aged APP23 transgenic mice. *Glia* 2008; **56**: 1438–1447.
32. Gaikwad S, Larionov S, Wang Y *et al.* Signal regulatory protein-β1: a microglial modulator of phagocytosis in Alzheimer's disease. *Am J Pathol* 2009; **175**: 2528–2539.
33. Moestrup SK, Møller HJ. CD163: a regulated hemoglobin scavenger receptor with a role in the anti-inflammatory response. *Ann Med* 2004; **36**: 347–354.
34. Husemann J, Loike JD, Anankov R, Febbraio M, Silverstein SC. Scavenger receptors in neurobiology and neuropathology: their role on microglia and other cells of the nervous system. *Glia* 2002; **40**: 195–205.
35. Fujita D, Terada S, Ishizu H *et al.* Immunohistochemical examination on intracranial calcification in neurodegenerative diseases. *Acta Neuropathol* 2003; **105**: 259–264.

European Journal of Neurology 2010
doi:10.1111/j.1468-1331.2010.03311.x

SHORT COMMUNICATION

Nasu–Hakola disease with a splicing mutation of TREM2 in a Japanese family

Y. Numasawa[a], C. Yamaura[a], S. Ishihara[a], S. Shintani[a], M. Yamazaki[b], H. Tabunoki[c] and J.-I. Satoh[c]

[a]*Department of Neurology, Toride Kyodo General Hospital, Toride City, Ibaraki;* [b]*The 2nd Department of Internal Medicine, Nippon Medical School, Bunkyo-ku, Tokyo; and* [c]*Department of Bioinformatics and Molecular Neuropathology, Meiji Pharmaceutical University, Kiyose, Tokyo, Japan*

Keywords:
exon 3 skipping, Nasu–Hakola disease, PLOSL, transcriptome, TREM2 mutation

Received 28 September 2010
Accepted 18 November 2010

Background: Nasu–Hakola disease (NHD) is a rare autosomal recessive disorder, characterized by a combination of progressive presenile dementia and formation of multifocal bone cysts, caused by genetic mutations of DAP12 and TREM2, which constitute a receptor/adapter signaling complex expressed on osteoclasts, dendritic cells, macrophages, and microglia. No Japanese patients with TREM2 mutations have been reported previously.

Methods: We reported three siblings affected with NHD in a Japanese family. Amongst them, two died of NHD during the fourth decade of life. The analysis of genomic DNA, cDNA cloning, and western blot of lymphocyte proteins was performed on samples of the living patient. The transcriptome was studied in the autopsied brain of one patient.

Results: We identified a homozygous conversion of a single nucleotide T to C at the second position of intron 3 in the splice-donor consensus site (c.482+2T>C) of the TREM2 gene, resulting in exon 3 skipping and aberrant expression of truncated proteins. We identified 136 upregulated genes involved in inflammatory response and immune cell trafficking and 188 downregulated genes including a battery of GABA receptor subunits and synaptic proteins in the patient's brain.

Conclusions: This is the first report of a Japanese NHD family caused by a splicing mutation of TREM2 that induces both neuroinflammation and neurodegeneration.

Introduction

Nasu–Hakola disease (NHD; OMIM 221770), also designated polycystic lipomembranous osteodysplasia with sclerosing leukoencephalopathy (PLOSL), is a rare autosomal recessive disorder, characterized by a combination of progressive presenile dementia and formation of multifocal bone cysts [1]. The clinical course of NHD is divided into four stages: (i) the latent stage with normal early development, (ii) the osseous stage beginning at the third decade of life, characterized by pathological bone fractures, (iii) the early neuropsychiatric stage occurring at the fourth decade of life, presenting with a frontal lobe syndrome, and (iv) the late neuropsychiatric stage, characterized by profound dementia, and death usually by age 50 years [1].

Nasu–Hakola disease is caused by a structural defect in one of the two genes, DAP12 (TYROBP) or TREM2, both of which induce a clinicopathologically identical phenotype [2,3]. DAP12, expressed as a disulfide-bonded homodimer on NK cells, monocytes/macrophages, dendritic cells, osteoclasts, and brain microglia, constitutes a transmembrane adaptor that non-covalently associates with several cell-surface receptors, including TREM2, TREM1, NCR2 (NKp44), SIRPB1, and MDL1, and transmits activating or inhibitory signals depending on the avidity of their ligands. The TREM2/DAP12 complex regulates key signaling events involved in immune responses, differentiation of dendritic cells and osteoclasts, and phagocytic activity of microglia. Until present, 17 different NHD-causing mutations have been identified in

Correspondence: J.-I. Satoh, MD, PhD, Department of Bioinformatics and Molecular Neuropathology, Meiji Pharmaceutical University, 2-522-1 Noshio, Kiyose, Tokyo 204-8588, Japan (tel.: +81 42 495 8678; fax: +81 42 495 8678; e-mail: satoj@my-pharm.ac.jp).

either DAP12 or TREM2 [2,3]. DAP12 mutations are predominant in Finnish and Japanese, whilst TREM2 mutations are distributed widely. However, no NHD patients with TREM2 mutations have been previously found in Japan. In this study, we describe the first case of a Japanese NHD family caused by a splicing mutation of TREM2.

Methods

Mutation analysis

After written informed consent was obtained, high molecular weight genomic DNA was extracted from whole peripheral blood. The Ethics Committee of MPU approved this study. All five exons and 5′ and 3′ flanking regions of the TREM2 gene were amplified by PCR using primer sets following: exon 1, 5′caccgccttcataattcaccc3′ and 5′gactcctcctcccctctgtc3′; exon 2, 5′agtgggtggttctgcacac3′ and 5′gctccttcagggcaggattt3′; exon 3, 5′gctctagttgccttgtaatttgtagt3′ and 5′agtgtaatgacctgatccacatagga3′; and exons 4 and 5, 5′tcttccttcacgtgtctctcagcc3′ and 5′aaggcccatcccagggatggtgct3′. The purified PCR products were processed for direct sequencing on the 3730xl DNA Analyzer (Applied Biosystems, Foster City, CA, USA). cDNA and protein extract were prepared from peripheral blood mononuclear cells (PBMC). The junctional sequence of exons 3 and 4 or the sequence spanning the entire open-reading frame (ORF) and 5′ and 3′ flanking regions amplified by PCR of cDNA was cloned in the pcDNA4/HisMax-TOPO vector (Invitrogen, Carlsbad, CA, USA) and processed for sequencing analysis.

DNA microarray and molecular network analysis

Total RNA was isolated from a small piece derived from the fragmented bulk of autopsied frozen frontal lobe tissues of the patient 1. In parallel, we studied gene expression profile of the normal human frontal lobe RNA (636563; Clontech, Mountain View, CA, USA), pooled from unspecified regions isolated from four male/female Caucasians of ages 32–61 died of sudden death, serving as a control. The RNA integrity number (RIN) of total RNA on 2100 Bioanalyzer (Agilent Technologies, Palo Alto, CA, USA) was 6.1 for the control and 6.7 for the patient's sample, respectively. One hundred ng of total RNA was processed for microarray analysis with Human Gene 1.0 ST Array (Affymetrix, Santa Clara, CA, USA) containing 28 869 genes. The CEL file data were normalized by the robust multiarray average (RMA) method. When compared with gene expression levels in the control, the genes showing upregulation greater than fourfold or downregulation smaller than 0.1-fold were defined as differentially expressed genes. To identify biologically relevant molecular pathways, we utilized Ingenuity Pathways Analysis (IPA) tool (Ingenuity Systems). By uploading the list of Gene IDs and expression values, the network-generation algorithm identified focused genes integrated in a global molecular network with the score *P*-value reflecting the statistical significance of association between the genes and the networks by the Fisher's exact test.

Results

The Japanese NHD family

A 36-year-old woman (the patient 3; the index) was admitted to the hospital because of epileptic seizure. Her parents are consanguineous. The patient has three siblings. The eldest brother (the patient 1) developed intractable epileptic seizures at age 33 was diagnosed as having NHD, became bedridden, and died at age 39 because of decubital infection in a different hospital, where the autopsy was performed. The second elder brother (the patient 2) was also clinically diagnosed as NHD in another hospital, and lead to sudden death of an unknown cause at age 31. The elder sister at age 44 is currently healthy.

The patient 3 has been normal until age 34, when she gradually began to show personality change, characterized by laziness, lack of concentration and insight, and loss of judgment and social inhibitions. At age 36, she showed a sign of apathy and memory disturbance and was affected with generalized tonic-clonic seizures. On admission, she was postictal but neurologically normal except for diffuse hyperactive deep-tendon reflexes and occasional myoclonic jerks. She showed a profound decrease in the score (seven of 30) on examination of a revised version of Hasegawa's Dementia Scale.

X-ray examinations showed multifocal radiolucent lesions distributed in distal ends of humerus, radius, femur, tibia, and metatarsal bone (Fig. 1a). Brain CT revealed bilateral calcification of the basal ganglia (Fig. 1b). Brain MRI showed moderate atrophy of the frontotemporal cortex and marked dilatation of the lateral ventricle on a T2-weighted image (Fig. 1c). 99mTc-ECD SPECT showed moderate hypoperfusion in the frontotemporal cortex with preservation of the cerebral blood flow in the basal ganglia (Fig. 1d). An EEG displayed sporadic spike waves in diffuse slow activities. The routine laboratory examination of blood and cerebrospinal fluid was normal. All of neurological and radiological findings described earlier supported a clinical diagnosis of NHD.

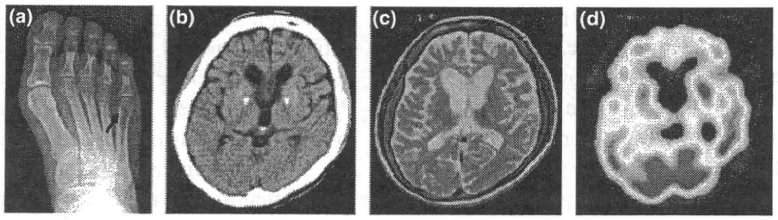

Figure 1 Neuroradiological features of the patient 3. (a) X-ray film. A cystic lesion in the fifth metatarsal bone (arrow). (b) Brain CT. High density lesions in the bilateral basal ganglia. (c) Brain MRI. Moderate atrophy of the frontotemporal cortex and marked dilatation of the lateral ventricle on an axial T2-weighted image (TR: 4500 ms, TE: 98 ms). (d) 99mTc-ECD SPECT. Moderate hypoperfusion in the frontotemporal cortex with preservation of the cerebral blood flow in the basal ganglia.

Identification of a splicing mutation in intron 3 of the TREM2 gene

In the patient 3, we identified a homozygous conversion of a single nucleotide T to C at the second position of intron 3 in the splice-donor consensus site (c.482+2T>C) of the TREM2 gene (Fig. 2a). No mutations were found in the DAP12 gene. The junctional sequence between exon 3 and exon 4 was not detected by PCR of cDNA of the patient 3 (Fig. 2b, lane 1). By western blot, a 38-kDa full-length TREM2 protein was identified in PBMC of a normal subject (Fig. 2c, lane 2), whereas 27-kDa and 24-kDa truncated TREM2 proteins were detected in the patient 3 (Fig. 2c, lane 1).

The cloning and sequencing of the TREM2 ORF verified exon 3 skipping in combination with deletion of exon 2 and/or exon 4, followed by emergence of the premature or original stop codons (Fig. S1, panels a–d). The exon 3-skipped genes are predicted to encode four distinct truncated proteins, composed of 157 amino acids (35-kDa), 135 amino acids (28-kDa), amino acids 40 (11-kDa), or 18 amino acids (0.5-kDa), tentatively named as variant 1, 2, 3, or 4, respectively. The wild-type full-length TREM2 protein consists of 230 amino acids, composed of a 13-amino acid signal peptide, followed by an 154-amino acid extracellular immunoglobulin superfamily (Ig-SF) domain pivotal for binding to the ligand, a 33-amino acid transmembrane (TM) domain essential for binding to DAP12, and a 30-amino acid cytoplasmic domain. InterProScan (http://www.ebi.ac.uk/Tools/InterProScan) search indicated that variants 1 and 2 have the Ig-SF domain but do not have the TM domain, whilst variants 3 and 4 lack both Ig-SF and TM domains, suggesting that all of these variants are non-functional. It remains unknown whether these variants expressed as truncated proteins produce a dominant negative effect on TREM2/DAP12 signaling.

Gene expression analysis of autopsied brain tissues

We again identified the c.482+2T>C mutation in the genomic DNA isolated from the brain of the patient 1. The transcriptome analysis of the brain identified totally 136 upregulated genes (Table S1) and 188 downregulated genes (Table S2). Macrophage/microglia marker genes, such as CD163, MSR1, and CD68,

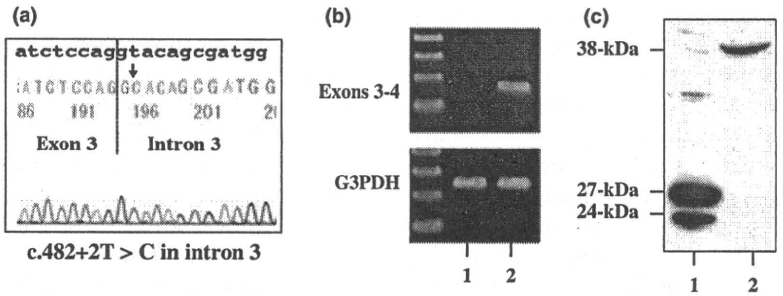

Figure 2 TREM2 mutation of the patient 3. (a) Direct sequencing. PCR and sequencing of all five exons and exon–intron boundaries of the TREM2 gene identified a homozygous conversion of a single nucleotide T to C in the splice-donor consensus site at the second position of intron 3 (c.482+2T>C). (b) The junctional sequence of exons 3 and 4. The junctional sequence of exons 3 and 4 of TREM2 (upper panel) and G3PDH (lower panel) amplified by PCR from cDNA of PBMC. The lanes (1, 2) represent (1) the patient and (2) normal subject. (c) TREM2 protein expression. Western blot of PBMC protein with anti-TREM2 antibody (HPA010917, Sigma). The lanes (1, 2) represent (1) the patient and (2) normal subject.

were greatly upregulated, whereas the genes encoding nine different GABA receptor subunits, such as GABRG2, GABRA1, GABRB2, GABRA2, GABRA4, GABRA3, GABRA5, GABRB3, and GABRB1, along with various synaptic components, such as SYT1, SNAP25, SV2B, SYNPR, SYT4, SYT13, SYN2, and SYT5, were coordinately downregulated. Top 10 genes, either upregulated or downregulated, are listed in Table 1. Upregulation of RGS1 and CD163 and downregulation of GABRG2 and SYT1 were validated by qRT-PCR analysis (Fig. S2). With respect to neuronal and glial marker genes, the fold change of gene expression levels in the patient's brain vs. the control is NEFH (neurons), 0.30; PVALB (GABA neurons), 0.18; GFAP (astrocytes), 2.57; MBP (oligodendrocytes), 1.60; and G3PDH (housekeeping gene), 0.63, suggesting marked loss of neurons with enhanced astrogliosis in the NHD brain at a terminal stage.

By IPA, the set of 136 upregulated genes constituted a highly complex network of 64 focused genes showing the most significant relationship with inflammatory response, cellular movement, and immune cell trafficking (P = 1.00E-116) (Fig. S3a), whilst 188 downregulated genes formed the network of 91 focused genes showing the most significant relationship with cell-to-cell signaling and interaction, nervous system development and function, and genetic disorder (P = 1.00E-168) (Fig. S3b).

Discussion

Here, we described the first report of a Japanese NHD family caused by a splicing mutation of TREM2. Three patients showed clinical features typical of NHD, and the patient 1 and the patient 3 exhibited a homozygous c.482+2T>C mutation inducing exon 3 skipping of the TREM2 gene. The identical mutation was reported previously in two patients of an Italian family [2–4]. Until present, 20 patients with 11 different TREM2 mutations have been reported worldwide, including one patient with G40T (Q14stop), four with C97T (Q33stop), one with G132A (W44stop), two with G233A (W78stop), one with 267delG (frameshift followed by premature termination), one with 313delG (frameshift followed by premature termination), two with T377G (V126G), one with A401G (D134G), two with G558T (K86N), two with c.482+2T>C (splicing mutation), or three with c.40+3delAGG at the third position of intron 1 in the splice-donor consensus site (splicing mutation) [2–6].

TREM2 is expressed exclusively in osteoclasts, dendritic cells, tissue-infiltrating macrophages, and a subpopulation of microglia, located in the Golgi complex and exocytic vesicles, on cell-surface membranes, and in part released extracellularly [7]. TREM2 expressed on mouse microglia plays a key role in tissue debris clearance and resolution of inflammation [8]. We

Table 1 Top 10 upregulated and downregulated genes in the brain of a Nasu–Hakola disease patient with TREM2 mutation

Rank	Fold change	Gene ID	Gene symbol	Gene description
Upregulated genes				
1	40.2	5996	RGS1	Regulator of G-protein signaling 1
2	13.3	9103	FCGR2C	Fc fragment of IgG, low affinity IIc, receptor for (CD32)
3	13.2	9332	CD163	CD163 molecule
4	12.9	312	ANXA13	Annexin A13
5	12.1	4640	MYO1A	Myosin IA
6	11.6	7852	CXCR4	Chemokine (C-X-C motif) receptor 4
7	11.5	118932	ANKRD22	Ankyrin repeat domain 22
8	10.7	84689	MS4A14	Membrane-spanning 4-domains, subfamily A, member 14
9	10.7	1610	DAO	D-amino acid oxidase
10	10.4	3606	IL18	Interleukin 18 (interferon-gamma-inducing factor)
Downregulated genes				
1	0.008	7447	VSNL1	Visinin-like 1
2	0.010	2566	GABRG2	Gamma-aminobutyric acid (GABA) A receptor, gamma 2
3	0.010	2554	GABRA1	Gamma-aminobutyric acid (GABA) A receptor, alpha 1
4	0.011	5999	RGS4	Regulator of G-protein signaling 4
5	0.011	6857	SYT1	Synaptotagmin 1
6	0.012	6616	SNAP25	Synaptosomal-associated protein, 25kDa
7	0.014	8507	ENC1	Ectodermal-neural cortex (with BTB-like domain)
8	0.016	114569	MAL2	Mal, T-cell differentiation protein 2
9	0.018	4753	NELL2	NEL-like 2 (chicken)
10	0.018	9899	SV2B	Synaptic vesicle glycoprotein 2B

The transcriptome of frontal lobe tissues of the patient 1 was studied using Human Gene 1.0 ST array (Affymetrix). When compared with the gene expression levels in the control, top 10 upregulated and downregulated genes are listed with fold change, Entrez Gene ID, gene symbol, and description. See Tables S1 and S2 for the entire list.

for the first time characterized the genome-wide transcriptome of the NHD brain, although the case, the control, and the region of the brain, possibly affecting gene expression profiles, are fairly limited because of restricted availability of the samples. We identified a panel of upregulated genes closely associated with inflammatory response and immune cell function, and downregulated genes related to the nervous system function, indicating a concurrence of neuroinflammatory and neurodegenerative events in NHD brains.

Acknowledgements

This work was supported by grants to J-IS from Research on Intractable Diseases, the Ministry of Health, Labour and Welfare, Japan (H22-Nanchi-Ippan-136), and the High-Tech Research Center Project (S0801043) and the Grant-in-Aid (C22500322), the Ministry of Education, Culture, Sports, Science and Technology (MEXT), Japan. The gene sequence data are registered in GenBank with the accession number AB601768, and the microarray data are available from Gene Expression Omnibus (GEO) under the accession number GSE25496.

Disclosure of conflict of interest

The authors declare no financial or other conflict of interests.

References

1. Bianchin MM, Capella HM, Chaves DL, *et al.* Nasu–Hakola disease (polycystic lipomembranous osteodysplasia with sclerosing leukoencephalopathy-PLOSL): a dementia associated with bone cystic lesions. From clinical to genetic and molecular aspects. *Cell Mol Neurobiol* 2004; **24:** 1–24.
2. Klünemann HH, Ridha BH, Magy L, *et al.* The genetic causes of basal ganglia calcification, dementia, and bone cysts: DAP12 and TREM2. *Neurology* 2005; **64:** 1502–1507.
3. Paloneva J, Manninen T, Christman G, *et al.* Mutations in two genes encoding different subunits of a receptor signaling complex result in an identical disease phenotype. *Am J Hum Genet* 2002; **71:** 656–662.
4. Salmaggi A, Maccagnano E, Musso A, Di Lena L, Paloneva J, Boiardi A. An Italian family with Nasu–Hakola disease. *J Neurol* 2003; **250:** 878–880.
5. Soragna D, Papi L, Ratti MT, Sestini R, Tupler R, Montalbetti L. An Italian family affected by Nasu–Hakola disease with a novel genetic mutation in the TREM2 gene. *J Neurol Neurosurg Psychiatry* 2003; **74:** 825–826.
6. Chouery E, Delague V, Bergougnoux A, Koussa S, Serre JL, Mégarbané A. Mutations in TREM2 lead to pure early-onset dementia without bone cysts. *Hum Mutat* 2008; **29:** E194–E204.
7. Sessa G, Podini P, Mariani M, *et al.* Distribution and signaling of TREM2/DAP12, the receptor system mutated in human polycystic lipomembraneous osteodysplasia with sclerosing leukoencephalopathy dementia. *Eur J Neurosci* 2004; **20:** 2617–2628.
8. Takahashi K, Rochford CD, Neumann H. Clearance of apoptotic neurons without inflammation by microglial triggering receptor expressed on myeloid cells-2. *J Exp Med* 2005; **201:** 647–657.

Supporting Information

Additional Supporting Information may be found in the online version of this article:

Figure S1. The c.482 + 2T > C mutation induces exon 3 skipping. The ORF of TREM2 amplified by PCR was cloned in the vector. Four distinct clones were processed for sequencing analysis. The panels (a–d) represent (a) variant 1 with deletion of exon 3, composed of 157 amino acids, (b) variant 2 with deletion of exons 3 and 4, composed of 135 amino acids, (c) variant 3 with deletion of exons 2 and 3, composed of 40 amino acids, and (d) variant 4 with deletion of exons 2, 3, and 4, composed of 18 amino acids. The stop codon is underlined in variants 2 and 4.

Figure S2. Validation of microarray data by qRT-PCR. The microarray data was validated by quantitative RT-PCR on LightCycler ST300 (Roche Diagnostics). The panels represent (a) RGS1, (b) CD163, (c) GABRG2, and (d) SYT1. The expression levels of each gene were standardized against those of G3PDH. Frontal lobe cDNA of NC (the normal control), NHD (the patient 1), ALS1 and ALS2 (two patients with amyotrophic lateral sclerosis), and AD1 and AD2 (two patients with Alzheimer disease) were analyzed.

Figure S3. Molecular network of 136 upregulated and 188 downregulated genes in the brain of a NHD patient with TREM2 mutation. By Ingenuity Pathways Analysis of brain transcriptome data of the patient 1, 136 upregulated genes constitute the network of 64 focused genes (red) that has the most significant relationship with inflammatory response, cellular movement, and immune cell trafficking (P = 1.00E-116) (panel a), whilst 188 downregulated genes constitute the network of 91 focused genes (green) that has the most significant relationship with cell-to-cell signaling and interaction, nervous system development and function, and genetic disorder (P = 1.00E-168) (panel b).

Table S1. The list of 136 upregulated genes in the brain of a NHD patient with TREM2 mutation.

Table S2. The list of 188 downregulated genes in the brain of a NHD patient with TREM2 mutation.

Please note: Wiley-Blackwell is not responsible for the content or functionality of any supporting materials supplied by the authors. Any queries (other than missing material) should be directed to the corresponding author for the article.

BmDJ-1 is a Key Regulator of Oxidative Modification in the Development of the Silkworm, *Bombyx mori*.

Hiroko Tabunoki[1*], Hiroaki Ode[1], Yutaka Banno[2], Susumu Katsuma[3], Toru Shimada[3], Kazuei Mita[4], Kimiko Yamamoto[4], Ryoichi Sato[5], Reiko Ishii-Nozawa[6], and Jun-ichi Satoh[1]

[1]Department of Bioinformatics and Molecular Neuropathology, Meiji Pharmaceutical University, Tokyo 204-8588, Japan, [2]The Center of Genetic Resources, University of Kyushu, Fukuoka 812-0053, Japan; [3]Department of Agricultural and Environmental Biology, Graduate School of Agricultural and Life Sciences; The University of Tokyo, Tokyo 113-8657, Japan; [4]Insect Genome Laboratory, National Institute of Agrobiological Sciences, Tsukuba 305-8634, Japan; [5]Bio-Applications and Systems Engineering, Tokyo University of Agriculture and Technology, Koganei, Tokyo 184-8588, Japan; [6]Department of Clinical Pharmacology, Meiji Pharmaceutical University, Tokyo 204-8588, Japan

*Address correspondence to: Hiroko Tabunoki, Department of Bioinformatics and Molecular Neuropathology, Meiji Pharmaceutical University, 2-522-1 Noshio, Kiyose, Tokyo 204-8588, Japan. Tel: +81-424-95-8679, Fax: +81-424-95-8679, E-mail: tabunoki@my-pharm.ac.jp

Abstract

We cloned cDNA for the *Bombyx mori* DJ-1 protein (BmDJ-1) from the brains of larvae. BmDJ-1 is composed of 190 amino acids and encoded by 672 nucleotides. Northern blot analysis showed that BmDJ-1 is transcribed as a 756–bp mRNA and has one isoform. Reverse transcriptase (RT)-PCR experiments revealed that the BmDJ-1 was present in the brain, fatbody, Malpighian tuble, ovary and testis but present in only low amounts in the silkgland and hemocyte of day 4 fifth instar larvae. Immunological analysis demonstrated the presence of BmDJ-1 in the brain, midgut, fatbody, Malpighian tubule, testis and ovary from the larvae to the adult. We found that BmDJ-1 has a unique expression pattern through the fifth instar larval to adult developmental stage. Based on the lowest endogenous expression of BmDJ-1 in day 3 and 4 fifth instar larvae, we selected this stage for assessing the anti-oxidative function of BmDJ-1 using rotenone (ROT). Administration of ROT to day 3 fifth instar larvae together with exogenous (BmNPV-BmDJ-1 infection for 4 days in advance) BmDJ-1, produced significantly lower 24-h mortality in BmDJ-1 groups than in the control. 2D-PAGE revealed an isoelectric point (pI) shift to an acidic form for BmDJ-1 in BmN4 cells upon ROT stimulus. Among the factors examined for their effects on expression level of BmDJ-1 in the hemolymph, nitric oxid (NO) concentration was identified based on dramatic developmental stage-dependent changes. Administration of isosorbide dinitrate (ISDN), which is an NO donor, to BmN4 cells produced increased expression of BmDJ-1 compared to the control. These results suggest that NO controls BmDJ-1 expression in the cell and serves as a development modulation factor in *B. mori*.

Introduction

The protein DJ-1 is ubiquitously expressed in cells and it is highly conserved across a wide variety of organisms, showing moderate sequence identity with heat shock protein 31 (HSP31) chaperones and ThiJ/Pfpl cysteine proteases (1). Mutated forms of DJ-1 are known to cause early onset autosomal recessive juvenile Parkinson's disease (PD), and many studies have demonstrated a neuro-protective role of DJ-1. DJ-1, which is encoded by PARK7, is a multi-functional protein that plays roles in chaperoning, RNA-binding, SUMOlylation, apoptosis, and protease activity (2).

Additionally, DJ-1 is induced by oxidative modification and is rapidly oxidized at position Cys 106 (3). Oxidative modification leads to mitochondrial damage in cultured cells exposed to 1-methyl-4-phenyl-1,2,3,6 tetrahydropyridine (MPTP), 6-hydroxydopamine (6-OHDA), paraquat (PQ), and rotenone (ROT), which inhibit the mitochondrial electron transfer chain of mitochondrial complex I (4). These compounds enhance production of reactive oxygen species (ROS) and reduce production of ATP, resulting in mitochondria dysfunction (5). DJ-1 seems to directly scavenge free radicals from mitochondria in response to these oxidative stresses. MPTP, 6-OHDA, PQ, and ROT are used to produce PD models in rats and *Drosophila* and to analyze the pathology of PD (6,7).

DJ-1 has a dimer structure, and the L166P mutation produces structural perturbation that causes the protein to be ubiquitinated and susceptible to degradation by the 26S proteasome, significantly reducing its half-life *in vivo* (8,9). L166P DJ-1 forms unstable dimers with disrupted protein folding and function (10). The C106A mutation results in a loss-of-function of DJ-1 protease and chaperone activity (11,12). However, the precise pathology due to mutations and species-specific biological functions of DJ-1 remain unclear.

The silkworm, *Bombyx mori*, a Lepidopteran insect, has been utilized as a model system for basic science research because of its well-characterized genome, availability of various genetic mutants, and the development of transgenic, RNAi, and microarray technologies (13, 14, 15, 16, 17). The complete silkworm genome has approximately 18,510 genes, including a substantial number of mammalian orthologs (13, 16).

In the present study, we cloned the silkworm *B. mori* DJ-1 ortholog (BmDJ-1), clarified its expression pattern during development, and examined its anti-oxidative function. BmDJ-1 is a newly identified member of the DJ-1 family and is a growth-associated protein that is altered with development in *B. mori*.

Results

Molecular cloning of BmDJ-1

Amplifying BmDJ-1 by RT-PCR with 5' RACE using gene-specific primers from *B. mori* larvae brain cDNA produced an 86-bp product. The Kozak consensus sequence AAAATGAAG (18) was found to be present at the site of translation initiation determined using NetStart software (19). Therefore, we determined that the cDNA encoded a putative 5'-untranslated sequence of 95 bp, an ATG start site, and an open reading frame (ORF) at position 96 extending to position 668. The deduced ORF of BmDJ-1 was composed of 672 nucleotides comprising 190 amino acids, had a molecular weight of 20,113 Dalton, and a putative isoelectric point (pI) of 5.15.

A computer search of the SMART database (http://smart.embl-heidelberg.de/) revealed that BmDJ-1 contained a DJ-1_PfpI domain at position 31T-173T. We identified the location of the BmDJ-1 gene in scaffold 2995719-2998746 of chromosome 23 at the splitting of 5 blocks by linkage mapping 28 chromosomes by SNP markers (20).

A BLAST search showed that BmDJ-1 has 50% amino acid sequence identity to *D. rerio* DJ-1 (NCBI gene ID:449674) and *D. melanogaster* DJ-1 beta (NCBI gene ID:43652); 47% amino acid sequence identity to *H. sapiens* (NCBI gene ID:11315), *X. tropicalis* (NCBI gene ID:548568), *G. gallus* (NCBI gene ID:395227), *B. taurus* (NCBI gene ID:511268), and *R. novaltis* (NCBI gene ID:117287) DJ-1; 46% amino acid sequence identity to *C. elegans* (NCBI gene ID:183625) and *M. musculus* (NCBI gene ID:57320) DJ-1; and 45% amino acid sequence identity to *D. melanogaster* DJ-1 alpha (NCBI gene ID:36543). An alignment of the deduced BmDJ-1 amino

acid sequences and DJ-1 orthologs from other species using CLC Work Bench 3.2.3 showed that the BmDJ-1 protein sequence contains all of the conserved Cys and Leu residues (Fig. 1-A black asterisks).

The phylogenetic tree placed *D. melanogaster* DJ-1 and BmDJ-1 into a distinct cluster (Fig. 1-B).

BmDJ-1 mRNA is expressed in various tissues in fifth instar larvae

Northern blot analysis revealed that there is a single transcription product for BmDJ-1 with a size of 756 bp (Fig. 2A).

We used RT-PCR to investigate the expression profile of BmDJ-1 mRNA in various tissues. BmDJ-1 showed high expression in the brain, fatbody, Malpighian tubule, ovary, and testis (Fig. 2B, upper panel lanes 2, 5-8) and low expression in the midgut, silkgland, and hemocyte (Fig. 2B, upper panel lanes 3, 4, 9).

Specificity of antibody against BmDJ-1

We examined the utility of anti-BmDJ-1 antibodies raised against the recombinant Xpress-tagged BmDJ-1 to identify BmDJ-1. Anti-BmDJ-1 antibody reacted with both recombinant BmDJ-1 protein as a 25-KDa band and BmDJ-1 in the cell and tissue lysate from *B. mori* as a 20-KDa band. In contrast, BmDJ-1 antibodies did not recognize recombinant carotenoid binding protein (CBP) from *B. mori* tagged with GST (21) and HEK 293 cell lysate (Fig. 3, lanes 1 and 4). The molecular weight of the recombinant BmDJ-1 protein (Fig. 3, lanes 2 and 3) was slightly greater than the endogenous BmDJ-1 protein (Fig. 3, lanes 5 and 6), excluding the possibility of non-specific binding to the Xpress tag.

Identification of developmental stage and tissue-specific expression patterns of BmDJ-1 by immunoblotting

Distribution of BmDJ-1 expression by developmental stage and tissue is shown in Figure 4. Whole body expression is roughly equal for all larval instars, pupae, and adults (Fig. 4A, lanes 1-7). Moreover, equal amounts of BmDJ-1 are found in the brains of fifth instar larvae, pupae, and adults, but it is slightly increased in larvae (Fig. 4B, lanes 8-10). BmDJ-1 expression showed various patterns from day 0 fifth instar larvae to adult for these tissues (Fig. 4C: midgut, fatbody, Malpighian tubule, ovary, and testis) with the lowest expression levels of BmDJ-1 in all tissues in day 3 and 4 fifth instar larvae (Fig. 4C panels d, e). Expression was also decreased in the midgut of day 11 fifth instar larvae (Fig. 4C panel l, lane 1) and the fatbody of day 1 pupae (Fig. 4C panel o, lane 2). Expression levels in fifth instar larvae increased from day 5 to 7 (Fig. 4C panel f-h) and the highest expression levels for the fat body, Malpighian tubule, testis, and ovary were on pupal stage day 4 (Fig. 4C panel q). Therefore, BmDJ-1 showed a unique expression pattern day-to-day from day 0 fifth instar larvae to the adult developmental stages.

The pI of BmDJ-1 shifted acidic by ROT stimulation

Treatment of BmN4 cells with 50 μM ROT produced a shift in the pI to acidic, as shown on 2D-PAGE and immunoblotting (Fig. 5).

BmDJ-1 overexpression in larvae causes resistance to ROT

ROT was used to produce an oxidative stress in order to examine the effect of exogenous BmDJ-1 protein. As endogenous expression of BmDJ-1 is lowest in day 3 and 4 fifth instar larvae, the lethal dose (LD) of ROT for day 3 fifth instar larvae was determined to be 10.1 μg/g (LD50; 95% CI, 6.02-17.4) (Fig. 6). Based on computer simulations of reactivity using SAS software, we determined the optimal ROT concentration for further testing of the protective effects of BmDJ-1 to be 20 μg/g.

A BmDJ-1 overexpressing silkworm produced by injecting day 0 fifth instar larvae with recombinant BmNPV-BmDJ-1 virus showed significantly decreased mortality following intrahemocoelical injection of 20 μg/g ROT after 4 days (day 3 fifth instar larvae). For three experiments, the BmDJ-1 group mortality of 38, 27, and 15% was significantly lower than mortality rates of the blank vectors (control) of 81, 93, and 90%, respectively ($P<0.01$, <0.001, <0.001, respectively; Table. 1).

We also confirmed virus-derived BmDJ-1 expression in the fatbodies of several insects after 1 day (24 h) and 4 days (day 4 fifth instar larvae) by RT-PCR and after 4 days by immunoblotting. Expression of blank-vector recombinant virus was detected as a 300-bp band while virus-derived BmDJ-1 expression was detected as an 850-bp band. The BmDJ-1 expression was absent at 24 h but was detected at 96 h (Fig. 7A). Virus-derived BmDJ-1 protein was expressed at about 2-fold greater levels in non-treated groups than in ROT-treated groups after 4 days, and BmDJ-1 protein expression in blank virus-infected control groups was significantly decreased (Fig. 7B).

Expression of BmDJ-1 and NO concentration

The expression pattern of BmDJ-1 was stage-specific, reflecting the unique responses to oxidative stress. We examined some factors that might affect expression. NO concentration in the hemolymph was found to fluctuate from the fifth instar larva to adult (Fig. 8A) with high levels for day 0 and 6 fifth instar larvae and adults and gradually increasing NO concentration in the pupal stages. To test whether NO affects the expression of BmDJ-1, BmN4 cells were treated with 100 μM ISDN as an NO donor for 16 h. BmDJ-1 was detected in each sample by SDS-PAGE and immunoblotting with NO concentration (Fig. 8B) and BmDJ-1 expression (Fig. 8C) increased compared to the control (0.1% ethanol).

Discussion

Throughout its evolutionary history, DJ-1 shows a highly conserved amino acid sequence. Characterization of the *B. mori* variant, BmDJ-1, by cDNA cloning from the brains of the fifth instar larvae shows the presence of Cys and Leu, which are key residues for the function of DJ-1.

On a phylogenetic tree of DJ-1 proteins, two orthologs of *D. melanogaster* DJ-1α and DJ-1β, and BmDJ-1 placed in distinct clusters. *D. melanogaster* DJ-1α is most highly expressed in the testis from the pupal stages to adult, and DJ-1β is expressed in almost all tissues from embryo to adult. Loss-of-function DJ-1β mutant flies are sensitive to oxidative modification from H_2O_2 and paraquat, although the role played by DJ-1α remains unclear (22). Thus, these two *D. melanogaster* DJ-1s appear to have distinct functions.

In contrast, BmDJ-1 exists as a single isoform based on the single 756-bp transcript and only one band for BmDJ-1 on northern blot assay. The EST database (SilkBase; http://morus.ab.a.u-tokyo.ac.jp/cgi-bin/index.cgi) shows two distinct EST clones (data not shown). While BmDJ-1 may exist as several kinds of splice variants, this could not be clarified in this study.

BmDJ-1 demonstrated resistance to oxidative stress by ROT

DJ-1 has been reported to play a role in anti-oxidative stress by several independent groups. We confirmed that BmDJ-1 changes to an acidic form that is affected by ROT treatment in BmN4 cells (Fig. 5), indicating a response to oxidative stress.
In exogenous tests of BmDJ-1 with ROT, the mortality rate of individuals with BmDJ-1 is significantly decreased in the presence of ROT treatment, while the control groups remain extremely sensitive. It has been reported that the start of protein synthesis for BmNPV is 24 h after infection and that the protein expression level peaks at 96 h (23). Endogenous protein synthesis stopped at 24 h. Immunoblotting at 96 h showed that virus-derived BmDJ-1 protein expression was significantly increased and virus-infection control group of BmDJ-1 protein expression was significantly decreased. Our findings of virus-derived BmDJ-1 expression after 96 h corroborates those results and suggests that BmDJ-1 overexpression improves the survival of silkworm larvae treated with ROT.

BmDJ-1 expression controlled with NO

BmDJ-1 showed a tissue-specific expression pattern that indicates unique responses to oxidative stress. We found that NO was a oxidative stressor in *B. mori* that could be modulated by BmDJ-1.

The BmDJ-1 expression pattern in tissues in this study suggested that BmDJ-1 expression correlates to the hemolymph NO concentration, which showed day-to-day fluctuation from fifth instar larvae to adult (Figs. 4C and 8A). Moreover, the expression of BmDJ-1 was increased and the pI shifted acidic due to exposure to an NO donor (data not shown). These result showed that BmDJ-1 was oxidized and its expression was regulated by NO.

Choi et al. (24) reported that the nitric oxide synthease (NOS) gene in *B. mori* shows the highest expression in Malpighian tubule in day 7 fifth instar larvae, suggesting that NO might be related to *B. mori* metamorphosis. Inoue et al. (25) reported that administration of ISDN, an NO donor, to the beetle *Homoderus mellyi parry* rapidly progresses pupation. Conversely, the administration of carnitine, which suppresses apoptosis of cells in larval beetles, extended the larval developmental period and generated huge adult beetles. These observations implicate NO in the mechanism of metamorphosis as an apoptosis initiator, though the underlying process remains unclear.

In *B. mori*, apoptosis is the principal mechanism for dynamic remodeling of the body structure during metamorphosis. Apoptosis mainly occurs during the pupal developmental period during which the restructuring produces the adult body. In our observation, the highest expression levels of BmDJ-1 occur in the day 4 pupae, which coincide with apoptosis and the apparent melting of the body. BmDJ-1 might be involved in the elimination of NO in metamorphosis.
Although DJ-1 protein acts as a controller caspase activation to alter self expression level in the apoptotic pathway (26), we cannot determine a direct relationship between BmDJ-1 and NO generation in metamorphosis based on these experiments.

In future studies, we will investigate whether BmDJ-1 directly regulates NO in metamorphosis.

Materials and Methods

Ethics statement- The study protocol for the experimental use of the animals was approved by the Ethics Committee of Meiji Pharmaceutical of University. Approval ID of 2004.

Insects- The hybrid strain Kinshu x Showa was supplied from Ueda-Sha Co. Ltd., Nagano, Japan. Individuals were reared on the artificial diet Silkmate 2S (NOSAN, Tsukuba, Japan), and kept at 25°C on a 12 h light/12 h dark daily cycle.

Cell culture- An established silkworm cell line, BmN4 (NOSAN), was maintained at 25°C in TC-100 medium (NOSAN) supplemented with 10% fetal bovine serum and Antibiotic-Antimycotic (Invitrogen, Carlsbad, CA, USA).

Molecular cloning of BmDJ-1- We first searched the *B. mori* expressed sequence tag (EST) database on KAIKOBLAST (kaikoblast.dna.affrc.go.jp) using the *Drosophila melanogaster* DJ-1 alpha (NM_137072) or beta (NM_143568) sequence as a query, and identified the EST clone NRPG1136, which did not overlap the 5' end of the coding region of the *B. mori* DJ-1 gene (BmDJ-1). The entire coding sequence was determined using total RNA extracted from the brains of day 3 fifth instar larvae by an RNeasy mini kit (Qiagen, Valencia, CA, USA). DNase-treated total RNA was processed for cDNA synthesis using oligo(dT)12-18 primers and SuperScript II reverse transcriptase (Invitrogen), and cDNA was amplified by PCR using Pfu Turbo DNA polymerase (Stratagene, La Jolla, CA, USA) and the primers 5'-TCAAGAACAATGAGCAAGTCTGCG-3' and 5'-TAATATTAGTACTGCGAGATTAAC-3'. The amplified products were cloned into a cloning vector p3T (MoBiTec, Göttingen, Germany). The purified vectors were processed for sequencing by the dideoxynucleotide chain termination method on an ABI PRIZM 3100 Genetic Analyzer (Applied Biosystems, Tokyo, Japan).

5'-Rapid Amplification of cDNA ends- The 5'-terminal cDNA ends were amplified using the SMART RACE cDNA Amplification kit (Clontech, Mountain View, CA, USA) according to the supplier's instructions with primers 5'-GCCAGCTAGAGTAACTGTTACCCC-3' and 5'-AGTCACTTGCCTTGAGCACAGCAC-3'. The amplified products were cloned into a p3T vector for sequencing.

Deduced amino acid sequences, were aligned and phylogenetic trees and homology analyses were done using BLAST (blast.genome.jp), CLC Free Workbench ver 3.2.3 (CLC Bio, Aarhus, Denmark), and Genetyx ver 9.0 (Genetyx Co., Tokyo, Japan).

Recombinant protein- The ORFs of BmDJ-1 were amplified by PCR using PfuTurbo DNA polymerase and primers 5'-AGCAAGTCTGCGTTAGTGAT-3' and 5'-TTAGTACTGCGAGATTAACA-3'. Products were cloned into a prokaryotic expression vector pTrcHis-TOPO with a TOPO TA cloning kit (Invitrogen) and expressed in *E. coli* as fusion proteins with N-terminal Xpress tags. The nucleotide sequence was confirmed by sequencing. Recombinant BmDJ-1 expressed in *E. coli* was purified with HIS-Select spin columns (Sigma, St. Louis, MO, USA) according to methods described previously (27). A recombinant β-galactosidase (LacZ) fragment tagged with X-press included in the TOPO TA cloning kit was used as a negative control.

Immunology-The antibody for immunoblotting was raised in Japanese white rabbits by subcutaneous injection of the recombinant BmDJ-1 and Ribi adjuvant system (Corixa Co., Hamilton, MT, USA) mixture. The serum was stored at -80°C.

Immunoblotting- To identify the presence of BmDJ-1 in different tissues and cells, protein samples (5 μg) were separated on SDS-PAGE, transferred to nitrocellurose membranes using the method of Towbin *et al.* (28), and immunoblotted using rabbit anti-BmDJ-1 antibody and goat anti-rabbit IgG-conjugated horseradish peroxidase (HRP). The membranes were developed using a chemiluminescent substrate (Pierce, Rockford, IL, USA).

The tissue distribution of BmDJ-1 was determined for the following samples: the midgut, fatbody, Malpighian tubule, testis, ovary, and brain from day 0 fifth instar larvae, pupae, and adults. The distribution of BmDJ-1 from first instar larvae to adult on the whole body was also determined. All tissues were homogenized in RIPA lysis buffer composed of 50 mM Tris-HCl, pH 7.5, 150 mM NaCl, 1% Nonidet P40, 0.5% sodium deoxycholate, 0.1% SDS, and a cocktail of protease inhibitors (Sigma), followed by centrifugation at 10,000 × g for 15 min.

The protein concentration was determined by a Bradford assay kit (Pierce). Samples of supernatant (5 μg of protein) were separated by SDS-PAGE, transferred to nitrocellulose membranes, and immunoblotted with anti-BmDJ-1 antibody following the procedure described above.

Specificity of antibody against BmDJ-1- We examined the specificity of antibody against BmDJ-1 using following samples: 0.25 or 0.5 μg recombinant BmDJ-1 protein with xpress tag, 1 μg recombinant CBP protein with GST tag (21), 10 μg HEK293 cell lysate, BmN4 cell lysate and 10 μg larva brain lysate.

Northern blot analysis- Total RNA derived from the ovaries of day 4 fifth instar larvae were used. Total RNA (12 μg) was separated on a 1.5% agarose-6% formaldehyde gel and transferred to a nylon membrane. DIG-labeled probes were synthesized using the PCR DIG probe synthesis kit (Roche Diagnostics, Mannheim, Germany) according to the supplier's instructions with the primers 5'-CATTTGTGCTGCTTCCATAGCGTT-3' and 5'-CATTCCCTTTTCGACTTGATCGGC-3'. After pre-hybridization, the membranes were hybridized with the DIG-labeled probes at 54°C overnight. The specific reaction was visualized on Kodak X-OMAT AR X-ray films by the DIG chemiluminescence detection kit (Roche Diagnostics).

RT-PCR- Total RNA derived from the brain, midgut, fatbody, Malpighian tubule, testis, ovary, and hemocyte of day 4 fifth instar larvae was DNase-treated and processed for cDNA synthesis using oligo(dT)12–18 primers and SuperScript II reverse transcriptase (Invitrogen). cDNA was amplified by PCR using Taq DNA polymerase (Qiagen) and the primers 5'-CATTTGTGCTGCTTCCATAGCGTT-3' and 5'-CATTCCCTTTTCGACTTGATCGGC-3'. Amplification was carried out for 30 cycles of denaturing for 40 s at 94°C, annealing for 40 s at 50°C and extension for 90 s at 72°C. Amplified PCR products were separated by agarose gel, stained with ethidium bromide, and visualized under UV light.

Transfer plasmid and generation of recombinant virus- The ORF sequence of BmDJ-1 was amplified by PCR from brain cDNA as described above, with the primers 5'-GGGGTACCCCATGAGCAAGTCTGCGTTAGTGAT-3' and 5'-GGAATTCCAATATTAGTACTGCGAGATTAAC-3'. The amplified region was digested with EcoRI and KpnI and cloned into the baculovirus transfer pBK283 vector. Blank pBK283 vector was used as a control. For generating recombinant BmNPV, we used a Bom-EX kit (NOSAN) according to the supplier's instructions. The recombinant BmNPV nucleotide sequence was confirmed by sequencing using the primers 5'-ACTGTCGACAAGCTCTGTCC-3' and 5'-